Three-Dimensional Free Convection Boundary Layers in Porous Media Induced by a Heated Surface With Spanwise Temperature Variations

D. A. S. Rees
Department of Mechanical Engineering,
University of Bath,
Claverton Down,
Bath BA2 7AY,
United Kingdom
ensdasr@bath.ac.uk

In this paper we consider the effect of a nonuniform surface temperature distribution on the steady laminar free convection boundary layer flow induced by a vertical plate embedded in a fluid-saturated porous medium. The surface temperature profile exhibits sinusoidal variations in the spanwise (horizontal) direction, but the minimum temperature remains above or equal to that of the ambient medium. The resulting boundary layer flow is three-dimensional, and the governing equations are solved using a combination of a spanwise spectral decomposition and the Keller-box method. Detailed results in terms of the evolution of the rates of heat transfer and the developing thermal field are presented. The numerical work is supplemented by an asymptotic analysis valid far downstream where it is found that the effect of nonuniform heating becomes confined to a thin layer of uniform thickness embedded within the main growing boundary layer.

1 Introduction

The study of free convection heat transfer from uniform surfaces embedded in a saturated porous medium has attracted a great deal of interest from many investigators over the last two decades; see Nield and Bejan (1992) for a comprehensive review of this topic. Studies have centered on those cases where the thermal boundary conditions allow the use of similarity transformations to reduce the governing equations to a system of ordinary differential equations. In general, this means that the heated surface is plane and that the imposed temperature or surface heat flux satisfies a power-law distribution. However, in practice, surfaces are sometimes roughened intentionally in order to enhance the heat transfer. Roughened surfaces are encountered in several heat transfer devices such as flat-plate solar collectors and flat-plate condensers in refrigerators. Larger-scale surface nonuniformities are encountered in cavity wall insulating systems and grain storage containers. Similarly, nonuniformities in the boundary conditions in a plane surface may be obtained by the presence of a nonuniform heat source located nearby.

There is a growing body of literature devoted to this type of generic problem. There are now many papers dealing with boundary nonuniformities in porous channels: Riahi (1993, 1995, 1996) and Rees and Riley (1989a, b) and Rees (1990). But the first papers to study the effects of such nonuniformities on thermal boundary layer flow of a Newtonian (clear) fluid are those of Yao (1983) and Moulic and Yao (1989a, b). More recently, Chiu and Chou (1993) have extended this work to micropolar fluids, and Hossain et al. (1996) to a study of magnetohydrodynamic flow of a highly electrically-conducting fluid. In the area of convection in a porous medium, Rees and Pop (1994a, b, 1995a, b) have considered the effect of wavy surfaces on the otherwise self-similar free convection boundary layer flows. When a uniformly heated vertical surface exhibits surface waves, the resulting flow does in fact remain self-similar (Rees and Pop, 1994a), but when inertia effects are included, this property is lost (Rees and Pop, 1995a). However, when a vertical surface with a uniform heat flux has steady surface waves, the flow immediately becomes nonsimilar even in the absence of inertia effects (Rees and Pop, 1995b). In Rees and Pop (1994b) we considered very small amplitude undulations in a uniformly heated horizontal surface; in this case there exists the possibility of separated flow in the lee of the undulations and conditions were presented to indicate whether or not this would occur for any particular case.

All the papers quoted so far have been concerned with transverse nonuniformities where the boundary conditions are independent of the spanwise direction and, therefore, the resulting flow is two-dimensional. A more recent paper has considered the case of longitudinal surface waves (spanwise variations) on free convection from a vertical surface in a porous medium (Rees and Pop, 1996). Under a wide range of boundary conditions, the flow remains self-similar, but the authors showed that this is only true when the boundary layer thickness is asymptotically smaller than the spanwise wavelength of the nonuniformity. In particular, when the surface temperature is uniform, this means that nonsimilarity is first obtained at an $O(R)$ distance from the leading edge, where R is the porous medium Rayleigh number. In the present paper, we consider a uniform surface with an imposed surface temperature distribution which varies sinusoidally in the spanwise direction. Such a configuration could be supposed to model the presence of a hot water pipe immediately adjacent to a porous insulating cavity such as a double-skin wall of a house packed with a porous insulant, although we are unaware of experimental data against which to compare the present analyses. The resulting flow is three-dimensional, and we study the boundary layer flow using both numerical and asymptotic methods.

The formulation of the problem is given in Section 2, while the detailed description of the numerical method is contained in Section 3. The numerical results are presented in Section 4. Section 5 contains the asymptotic analysis for large distances from the leading edge where we show that the boundary layer

Contributed by the Heat Transfer Division for publication in the JOURNAL OF HEAT TRANSFER. Manuscript received by the Heat Transfer Division September 3, 1996; revision received April 11, 1997; Keywords: Flow Nonuniformity; Natural Convection; Porous Media. Associate Technical Editor: K. Vafai.

splits into a two-layer structure. This type of behavior, where the main boundary layer has a constant thickness near-wall layer embedded within it, also arises in other contexts. Another example of such a two-layer structure arises in the study of the influence of boundary (Brinkman) effects on the vertical free convection boundary layer in a porous medium, as discussed by Kim and Vafai (1989). Finally, the results are discussed briefly in Section 6.

2 Formulation of the Problem

We consider the laminar free-convection boundary layer flow induced by a vertical heated semi-infinite surface embedded in a fluid-saturated porous medium. Attention is given to the case where the surface temperature exhibits sinusoidal variations in a spanwise direction about a mean value which is above the temperature of the ambient medium. The resulting flow is three-dimensional and nonsimilar.

In this paper dealing with three-dimensional boundary layer flows, we assume that the porous medium is isotropic, uniform, and nondeformable, that the fluid and the porous matrix are in local thermal equilibrium, and that inertia, boundary, and dispersion effects are absent. All of these assumptions may be relaxed in future work. Additionally, the flow is laminar and steady; this is a very reasonable assumption given the recent papers by Rees (1993) and Lewis et al. (1995) which show that the vertical free convection boundary layer induced by a uniformly heated surface in a porous medium is stable. It is possible that boundary effects may modify this qualitative behavior, for in the analagous problem of convection in a vertical channel with sidewall heating (the Darcy-Bénard problem rotated through 90 deg), Kwok and Chen (1987) showed that uniform Darcy-Brinkman flow is susceptible to instability, whereas the pure Darcy-flow case is stable (see Gill, 1969 and Lewis et al., 1995).

The nondimensional equations of motion governing steady Darcy-Boussinesq free convection flow for this problem are

$$\frac{\partial u}{\partial x} + \frac{\partial v}{\partial y} + \frac{\partial w}{\partial z} = 0 \tag{1a}$$

$$u = -\frac{\partial p}{\partial x} + R\theta \tag{1b}$$

$$v = -\frac{\partial p}{\partial y}, \quad w = -\frac{\partial p}{\partial z} \tag{1c, d}$$

$$\nabla^2\theta = u\frac{\partial \theta}{\partial x} + v\frac{\partial \theta}{\partial y} + w\frac{\partial \theta}{\partial z} \tag{1e}$$

where we have used the same nondimensionalisation as Rees and Pop (1994a). In (1), x, y, and z are Cartesian coordinates corresponding, respectively, to the streamwise (i.e., upwards), cross stream (i.e., normal), and spanwise directions. The corresponding velocity fluxes are (u, v, w). In Eqs. (1), p is the pressure, θ is the temperature, and ∇^2 is the three-dimensional Laplacian operator. The porous medium Rayleigh number, R, is defined as

$$R = \frac{\rho g \beta d K \Delta T}{\mu \kappa} \tag{2}$$

where ρ is a reference density, g is gravity, β is the coefficient of cubical expansion, μ is the fluid viscosity, and κ is the thermal diffusivity of the saturated medium. In (2), ΔT is the difference between the mean surface temperature and the ambient temperature, K is the permeability, and d is a lengthscale associated with the surface variations, and is such that one full thermal wavelength is precisely $2\pi d$. The boundary conditions required to complete the specification of the problem are

$$v = 0, \quad \theta = 1 + a\cos z \quad \text{at} \quad y = 0, \tag{3a}$$

$$v \to 0, \quad \theta \to 0 \quad \text{as} \quad y \to \infty, \tag{3b}$$

where a is the amplitude of the surface wave. The three velocity components in (1) may be eliminated to obtain the pressure/temperature formulation

$$\nabla^2 p = R\frac{\partial \theta}{\partial x}, \quad \nabla^2\theta = R\theta\frac{\partial \theta}{\partial x} - \nabla p \cdot \nabla\theta \tag{4a, b}$$

subject to the boundary conditions

$$\frac{\partial p}{\partial y} = 0, \quad \theta = 1 + a\cos z \quad \text{at} \quad y = 0, \tag{4c}$$

$$\frac{\partial^2 p}{\partial y^2} \to 0, \quad \theta \to 0 \quad \text{as} \quad y \to \infty. \tag{4d}$$

Without the spanwise surface temperature variation, we recover the well-known Cheng and Minkowycz (1977) similarity solution for free convection from a uniformly heated vertical surface in a porous medium. Cheng and Minkowycz (1977) developed their solution in terms of a local Rayleigh number, a standard method of analysis since there is no natural length scale in the problem they considered. In the present analysis, the surface temperature wavelength provides such a length scale and, therefore, it proves most convenient to work in terms of the Rayleigh number based on this lengthscale. Thus, we can take the Cheng and Minkowycz similarity variable in the form

$$\eta = \frac{yR^{1/2}}{x^{1/2}}. \tag{5a}$$

Nomenclature

a = wave amplitude
d = spanwise dimensional lengthscale
f = similarity solution in (7)
g = gravitational acceleration
h = function defined in (7)
n = subscript
N = truncation level
j = subscript
p = pressure
P = near-wall pressure in asymptotic analysis
$R = \rho g \beta d K \Delta T/\mu\kappa$ = porous medium Rayleigh number
ΔT = reference temperature drop
u = streamwise flux velocity
v = cross-stream flux velocity
w = spanwise flux velocity
x = vertical or streamwise coordinate
y = horizontal or cross-stream coordinate
z = horizontal or spanwise coordinate
β = coefficient of thermal expansion
$\gamma = f''(0)$ in the solution of Eqs. (7)
η = similarity variable
θ = temperature
Θ = near-wall temperature in asymptotic analysis
λ = unknown coefficient
μ = dynamic viscosity
κ = effective thermal diffusivity
ρ = reference fluid density
σ = eigensolution exponent
ξ = scaled streamwise coordinate

The boundary layer is confined to regions where $\eta = O(1)$, and from both this observation and the definition of η in (5a), we see that when $x = O(1)$ the boundary layer thickness in terms of y is of magnitude $O(R^{-1/2})$. However, we are interested in how the spanwise variations affect the boundary layer flow. It is important, therefore, that the cross stream and spanwise diffusion effects balance in terms of their orders of magnitude. Since $z = O(1)$, we must have $y = O(1)$, and hence, from (5a), $\eta = O(1)$ implies that $x = O(R)$. Therefore, we define a new streamwise coordinate, ξ, using

$$\xi = \left(\frac{x}{R}\right)^{1/2} \tag{5b}$$

and introduce both this and (5a) into Eq. (4). As R is assumed to be asymptotically large, we retain only the leading order terms in each equation to obtain the following boundary layer equations:

$$\frac{\partial^2 p}{\partial \eta^2} + \xi^2 \frac{\partial^2 p}{\partial z^2} + \frac{1}{2}\eta \frac{\partial \theta}{\partial \eta} - \frac{1}{2}\xi \frac{\partial \theta}{\partial \xi} = 0, \tag{6a}$$

$$\frac{\partial^2 \theta}{\partial \eta^2} + \xi^2 \frac{\partial^2 \theta}{\partial z^2} + \frac{1}{2}\eta\theta \frac{\partial \theta}{\partial \eta} + \frac{\partial p}{\partial \eta}\frac{\partial \theta}{\partial \eta} + \xi^2 \frac{\partial p}{\partial z}\frac{\partial \theta}{\partial z} - \frac{1}{2}\xi\theta \frac{\partial \theta}{\partial \xi} = 0. \tag{6b}$$

We note in passing that the Cheng and Minkowycz (1977) similarity solution, which forms the solution of (6) when $a = 0$, may be written in the form

$$p = \int_0^\eta f(\alpha)d\alpha - \frac{1}{2}\eta f(\eta) \equiv h(\eta), \quad \theta = f'(\eta) \tag{7a, b}$$

where f is given by the equation

$$f''' + \tfrac{1}{2}ff'' = 0 \tag{7c}$$

subject to

$$f(0) = 0, \quad f'(0) = 1, \quad \text{and} \quad f'(\eta) \to 0 \quad \text{as} \quad \eta \to \infty. \tag{7d}$$

Here, primes denote differentiation with respect to η, and (7a) defines the function $h(\eta)$.

3 Numerical Solution Procedure

Equations (6) are parabolic in ξ, but at $\xi = 0$ they form a pair of ordinary differential equations. Without z-variations the most common approach to solving such parabolic systems in boundary layer flows is to use the Keller-box method (see Keller and Cebeci, 1971). The extra spatial dimension which is present here yields additional difficulties but there are at least three possible methods which could be used to solve Eqs. (6): (i) a full finite difference discretization with an implicit or semi-implicit discretization in ξ which is solved using Gauss-Seidel with multigrid acceleration at each value of ξ (such a scheme is not too great a modification from that used by Rees and Bassom (1993) to investigate boundary layer instabilities in porous media); (ii) a full finite difference discretization solved using multidimensional Newton-Raphson iteration by means of the block tri-diagonal (or Thomas) algorithm; or (iii) a spectral decomposition in the spanwise direction followed by the standard Keller-box method. Of these, the first and second methods are likely to be the least accurate unless very fine grids are used, and although the size of the problem obtained using (iii) is much larger than is usual for Keller-box applications, it was chosen as being the quickest to develop and, given the ease-of-use of nonuniform grids, potentially both the most accurate and the fastest to run. However, we also used method (i) with a large number of grid points to validate our Keller-box computations at the leading edge.

We expanded the solutions in the form

$$p = p_0(\xi, \eta) + 2\sum_{n=1}^{N} p_n(\xi, \eta)\cos nz,$$

$$\theta = \theta_0(\xi, \eta) + 2\sum_{n=1}^{N} \theta_n(\xi, \eta)\cos nz, \tag{8a, b}$$

where N is the truncation level. Substitution of (8) into (6) yields the following equations:

$$\frac{\partial^2 p_n}{\partial \eta^2} - n^2\xi^2 p_n = -\frac{1}{2}\eta\frac{\partial \theta_n}{\partial \eta} + \frac{1}{2}\xi\frac{\partial \theta_n}{\partial \xi}, \quad (n = 0, 1, \ldots, N) \tag{9a}$$

$$\frac{\partial^2 \theta_0}{\partial \eta^2} = -\frac{\partial p_0}{\partial \eta}\frac{\partial \theta_0}{\partial \eta} - \frac{1}{2}\eta\theta_0\frac{\partial \theta_0}{\partial \eta} + \frac{1}{2}\xi\theta_0\frac{\partial \theta_0}{\partial \xi} - 2\sum_{j=1}^{N}\left[\frac{\partial p_j}{\partial \eta}\frac{\partial \theta_j}{\partial \eta} + \frac{1}{2}\eta\theta_j\frac{\partial \theta_j}{\partial \eta} - \frac{1}{2}\xi\theta_j\frac{\partial \theta_j}{\partial \xi}\right] - 2\xi^2\sum_{j=1}^{N} j^2 p_j\theta_j, \tag{9b}$$

$$\frac{\partial^2 \theta_n}{\partial \eta^2} - n^2\xi^2\theta_n = \sum_{j=0}^{N-n}\left[-\frac{1}{2}\eta\left(\theta_j\frac{\partial \theta_{j+n}}{\partial \eta} + \theta_{j+n}\frac{\partial \theta_j}{\partial \eta}\right) - \left(\frac{\partial p_j}{\partial \eta}\frac{\partial \theta_{j+n}}{\partial \eta} + \frac{\partial p_{j+n}}{\partial \eta}\frac{\partial \theta_j}{\partial \eta}\right)\right] + \sum_{j=0}^{N-n}\frac{1}{2}\xi\left(\theta_j\frac{\partial \theta_{j+n}}{\partial \xi} + \theta_{j+n}\frac{\partial \theta_j}{\partial \xi}\right) - \sum_{j=1}^{N-n} j(j+n)\xi^2(p_j\theta_{j+n} + p_{j+n}\theta_j) + \sum_{j=1}^{n-1}\left[j(n-j)\xi^2 p_j\theta_{n-j} - \frac{\partial p_j}{\partial \eta}\frac{\partial \theta_{n-j}}{\partial \eta} - \frac{1}{2}\eta\theta_j\frac{\partial \theta_{n-j}}{\partial \eta} + \frac{1}{2}\xi\theta_j\frac{\partial \theta_{n-j}}{\partial \xi}\right], \quad (n = 1, 2, \ldots, N) \tag{9c}$$

where the final summation in (9c) only applies when the "upper" limit of the sum is not less than the "lower" limit.

Equations (9) form an arbitrarily large system of partial differential equations which can be discretized in the usual Keller-box style by first assigning grids in both the η and ξ directions. The η-grid used was nonuniform and consisted of 61 points lying between 0 and 20 with points concentrated near $\eta = 0$ to allow for the development of a near-wall layer. On the other hand, the ξ-grid was uniform and consisted of 1601 equally spaced points between 0 and 10. Equations (9) were reduced to first-order form in η, yielding a system of $4N + 4$ equations, and these were discretised using central differences based halfway between the η-gridpoints. Apart from at $\xi = 0$, where (9) forms a set of ordinary differential equations, a backward difference discretization in ξ was used; this was deemed necessary since central differences in ξ were found to yield pointwise oscillations reminiscent of those of the Crank-Nicholson method when the steplength is too large. These oscillations could be reduced in size by a very substantial decrease in the streamwise steplength, but the backward difference scheme, though for-

mally of first-order accuracy, yielded sufficiently accurate results and the solutions were free of oscillations.

If we include the boundary conditions in the reckoning, the discretized form of (9) has been transformed into a set of $(4N + 4)M$, nonlinear algebraic equations where M is the number of η-gridpoints. When the equations are arranged suitably, a multidimensional Newton-Raphson iteration scheme can be used to solve the resulting block tri-diagonal matrix/vector iteration equations. The specification of the iteration matrix, the Frechét derivative of the vector of algebraic equations, is exceedingly complicated, and should even one entry be in error, then it is highly likely to degrade seriously the performance of the Newton-Raphson method. Normally, this specification is given explicitly by the programmer. A safer and much quicker specification (though slightly slower computationally) is obtained using numerical differentiation. This technique has been used successfully very recently in another large-scale Keller-box analysis, that of boundary layer flow in a layered porous medium (Rees, 1996). Forward differences were used to obtain the iteration matrix, although high accuracy is not of great concern for this part of the solution methodology. Convergence of the Newton-Raphson procedure was deemed to have taken place when the maximum pointwise correction taken over all variables was less than 10^{-8}.

It is essential at this point to mention how the pressure boundary conditions at $\eta = \eta_{\max}$ were defined. Although $(4d)$ states that the second derivative of p must become zero, thereby allowing p to vary linearly at sufficiently large values of η, we find that this can be relaxed by setting $p = 0$ at $\eta_{\max}$. Referring to Eq. $(9a)$, the right-hand side tends to zero when η is large, and therefore the large-η asymptotic behavior of p_n is that it must be proportional to $e^{-n\xi}$. Thus, when $n \geq 1$, the boundary condition $p_n = 0$ is appropriate. When $n = 0$, a linear variation in p_0 can be allowed, but given the facts (i) that there is also a derivative boundary condition at $\eta = 0$, and (ii) that no ξ-derivatives in p appear in the boundary layer equations, we can impose $p_0 = 0$ at $\eta_{\max}$ with no effect on the overall solution except that the absolute pressure at each value of ξ is unknown. Thus, we compute the pressure relative to its absolute value at the edge of the boundary layer. Further, we have no need to know the absolute pressure, for the computation of v and w rely solely on pressure differences, and the streamwise velocity, u, is equal to $R\theta$ at leading order in R.

Initially, eleven Fourier modes were taken ($N = 10$ in (8)), but it was found that $N = 5$ gave almost indistinguishable results for all cases considered and also a much enhanced computational speed. Thus, we solved a 24th-order system, rather than a 44th-order system. Furthermore, we checked the accuracy of the solution at $\xi = 0$ by comparing directly with a finite difference solution of (6) at $\xi = 0$ using a suitably modified version of the code used by Rees and Bassom (1993). It is essential to note that, although z-derivatives are absent from the governing equations at $\xi = 0$, the surface temperature distribution, in conjunction with the nonlinear terms, serves to make the solution a function of z.

4 Numerical Results

Figure 1 shows the solution at $\xi = 0$ in the form of isotherms for various values of a, the surface temperature wave amplitude. It is important to note that since the velocities and pressure gradients (v, w, $\partial p/\partial y$ and $\partial p/\partial z$) must all balance in magnitude for large values of R, then $u = R\theta + o(R)$. Therefore, Fig. 1 also corresponds to vertical isovels. The aim of Fig. 1 is to display the way the wave amplitude, a, affects the temperature distribution at the leading edge. The main effect of having local hot spots is to cause the local thinning of the boundary layer, and vice versa. A close examination of Fig. 1 for the larger wave amplitudes appears, at first glance, to suggest that increasing the value of a causes the boundary layer to become thinner locally near a cold spot. However, this appearance is deceptive; for isotherm curves corresponding to, say, $\theta = 0.01$ and $\theta = 0.001$, they still indicate that the boundary layer is much thicker at the cold spot, but that it is also quite weak there because of the relatively small excess of the coldest surface temperature above that of the ambient medium.

The variation of the flow as ξ increases is presented in two forms. Firstly, in Fig. 2 we show how the isotherm field evolves at increasing distances from the leading edge. Secondly, the results of further computations are summarised in Fig. 3 in the form of the rates of heat transfer of the individual Fourier modes. Figure 2 shows isotherm plots for $a = 1.0$ at selected values of ξ. As ξ increases from zero, spanwise diffusion becomes increasingly important as the coefficients of the z-derivative terms in (6) are proportional to ξ^2. This has the effect of modifying the temperature field, and, in particular, of reducing the thickness of the boundary layer locally at the cold spots. Once more it is necessary to point out that isotherms corresponding to $\theta = 0.01$ and $\theta = 0.001$ show that the boundary layer is thicker at the cold spots than elsewhere. We find that by the time ξ takes the value 0.5, the boundary layer has essentially a uniform thickness as z varies and z-variations modify the profile only well within the boundary layer. In fact, we see that z-variations become confined to a decreasingly thin region close to the heated surface as ξ increases. Note that the expression "decreasingly thin" refers to the thickness of the near-wall layer in terms of η, but that the near-wall layer actually attains a uniform thickness in terms of y; this observation paves the way for the asymptotic analysis presented in the next section.

In Fig. 3 we show how the surface rate of heat transfer evolves downstream by considering the individual Fourier modes. Figure $3(a)$ shows how the value of $\theta_{0\eta}$ ($\eta = 0$) varies with ξ for various values of the wave amplitude. Here we see that the curves converge fairly quickly onto the value -0.444, which corresponds to an isothermal vertical surface (Cheng and Minkowycz, 1977). Much of the essential evolution, from the leading edge z-dependent solution to what is effectively the isothermal surface similarity solution (save for values of η close to zero), takes place in the interval $0 \leq \xi \leq 4$. The graph of $\theta_{1\eta}$ ($\eta = 0$) shown in Fig. $3(b)$ shows that, at large ξ, the variation of heat transfer is linear; this behavior is explained in the next section. Figures $3(c)$ and $3(d)$ show the evolution of the rate of heat transfer for the second and third modes, respectively. Both sets of curves display well-defined variations in $0 \leq \xi \leq 4$ although their amplitudes are smaller than those for modes 0 and 1. When $\xi > 4$, the rate of heat transfer has decayed very rapidly towards zero. Corresponding heat transfer curves for increasingly higher modes have decreasing maximum value, thereby justifying the choice of $N = 5$ mentioned earlier.

5 Asymptotic Analysis for Large Values of ξ

In this section, we present a brief analysis of the flow at large distances from the leading edge of the heated surface. Figure 2 has shown that the boundary layer splits into two very distinct regions: a main layer where $\eta = O(1)$ and there is no discernable z-variation, and a near-wall layer where $\eta \ll 1$ and z-variations are very evident. The near-wall layer may be shown to have a constant thickness (in terms of y) and it means that $\eta = O(\xi^{-1})$ in this region. Given that $\eta = y/\xi$, it is a simple matter to reduce Eqs. (6) to ones involving only y, z, and ξ. In the near-wall region we shall use P and Θ as the notation for pressure and temperature, respectively, and in both regions we expand the solution as an inverse power series in ξ. Let

$$\begin{pmatrix} p \\ \theta \end{pmatrix} = \begin{pmatrix} p^{(0)}(\eta) \\ \theta^{(0)}(\eta) \end{pmatrix} + \xi^{-1}\begin{pmatrix} p^{(1)}(\eta) \\ \theta^{(1)}(\eta) \end{pmatrix} + \xi^{-2}\begin{pmatrix} p^{(2)}(\eta) \\ \theta^{(2)}(\eta) \end{pmatrix} + \ldots, \quad (10a)$$

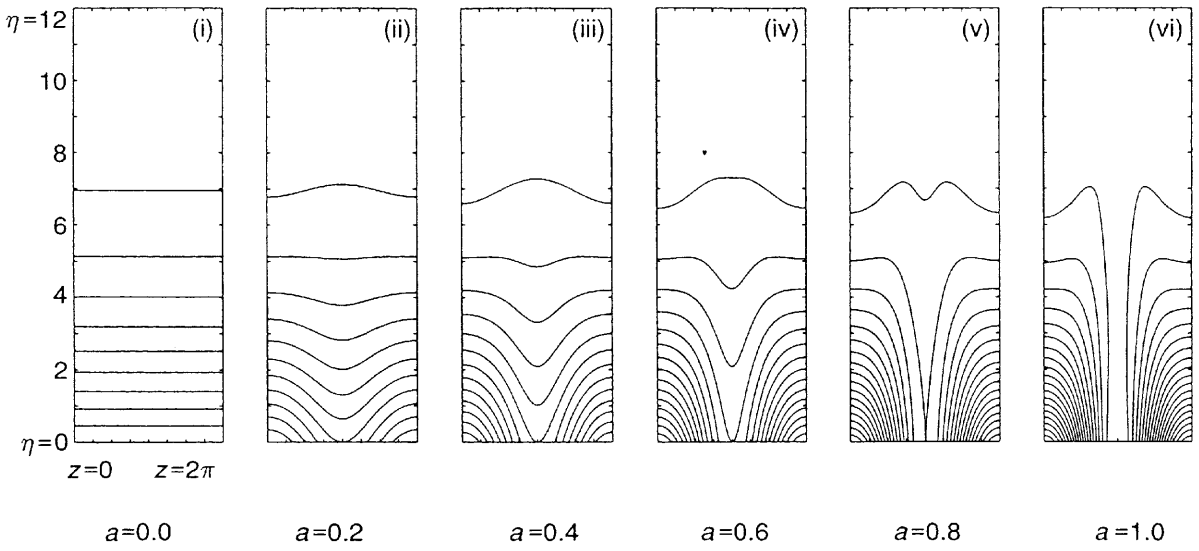

Fig. 1 The isotherms at $\xi = 0$ corresponding to various surface temperature wave amplitudes: (i) $a = 0$; (ii) $a = 0.2$; (iii) $a = 0.4$; (iv) $a = 0.6$; (v) $a = 0.8$; (vi) $a = 1.0$. All isotherm plots in this paper have the isotherms plotted at intervals of 0.1.

$$\begin{pmatrix} P \\ \Theta \end{pmatrix} = \begin{pmatrix} P^{(0)}(y) \\ \Theta^{(0)}(y) \end{pmatrix} + \xi^{-1}\begin{pmatrix} P^{(1)}(y) \\ \Theta^{(1)}(y) \end{pmatrix} + \xi^{-2}\begin{pmatrix} P^{(2)}(y) \\ \Theta^{(2)}(y) \end{pmatrix} + \ldots . \quad (10b)$$

The equations governing P and Θ into which (10b) will be substituted are

$$\frac{\partial^2 P}{\partial y^2} + \frac{\partial^2 P}{\partial z^2} - \frac{1}{2\xi}\frac{\partial \Theta}{\partial \xi} = 0, \quad (11a)$$

$$\frac{\partial^2 \Theta}{\partial y^2} + \frac{\partial^2 \Theta}{\partial z^2} + \frac{\partial P}{\partial y}\frac{\partial \Theta}{\partial y} + \frac{\partial P}{\partial z}\frac{\partial \Theta}{\partial z} - \frac{1}{2\xi}\Theta\frac{\partial \Theta}{\partial \xi} = 0. \quad (11b)$$

At large values of ξ, the flow in the main part of the boundary layer is generated by the mean temperature drop between the surface and the ambient medium, and it is easily shown that the solutions for $p^{(0)}$ and $\theta^{(0)}$ are given by the expressions for p and θ in (7). In the near-wall layer we find that

$$P^{(0)} = 0 \quad \text{and} \quad \Theta^{(0)} = 1 + ae^{-y}\cos z. \quad (12a, b)$$

The solution methodology proceeds by returning to the next order in the main layer, solving the resulting equations, obtaining the asymptotic matching conditions for the near-wall solution as $y \to \infty$, and finally, by solving the associated near-wall equations. The detailed analysis is straightforward but increasingly lengthy as successive terms are obtained. Before the results of our analysis are presented, however, it is important to note that the equations for the $O(\xi^{-2})$ terms in the main layer, i.e.,

$$\frac{d^2 p^{(2)}}{d\eta^2} + \frac{\eta}{2}\frac{d\theta^{(2)}}{d\eta} + \theta^{(2)} = 0, \quad (13a)$$

$$\frac{d^2\theta^{(2)}}{d\eta^2} + \frac{\eta}{2}\frac{d}{dy}(\theta^{(0)}\theta^{(2)}) + \left(\frac{dp^{(0)}}{dy}\frac{d\theta^{(2)}}{dy} + \frac{dp^{(2)}}{dy}\frac{d\theta^{(0)}}{dy}\right) + \theta^{(0)}\theta^{(2)} = 0, \quad (13b)$$

are homogeneous, but admit the eigensolutions

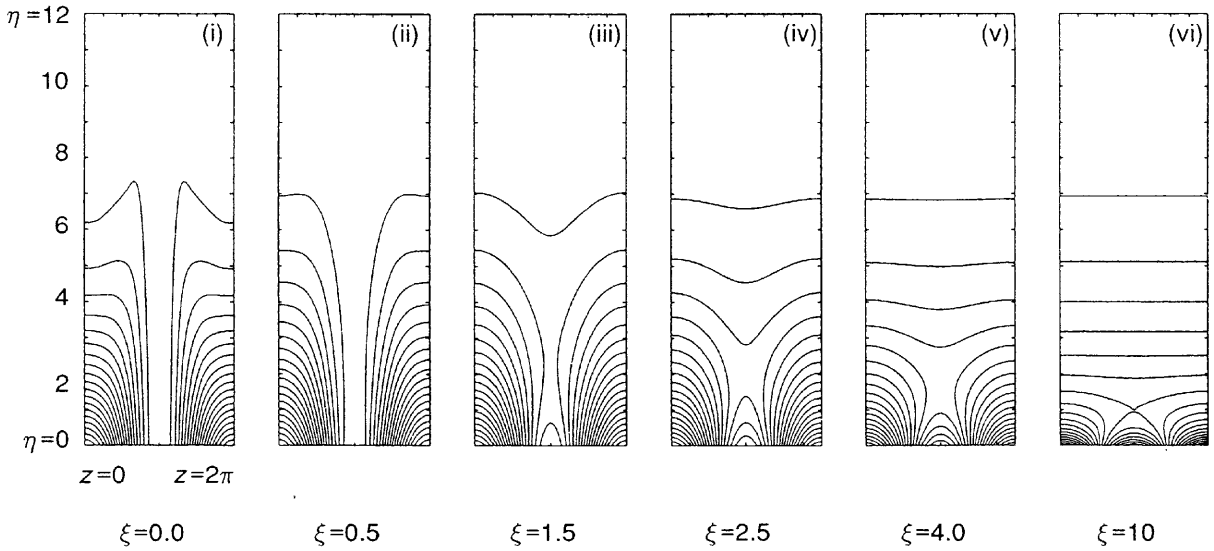

Fig. 2 The isotherms at various values of ξ corresponding to the surface temperature wave amplitude $a = 1.0$: (i) $\xi = 0$; (ii) $\xi = 0.5$; (iii) $\xi = 1.5$; (iv) $\xi = 2.5$; (v) $\xi = 4$; (vi) $\xi = 10$.

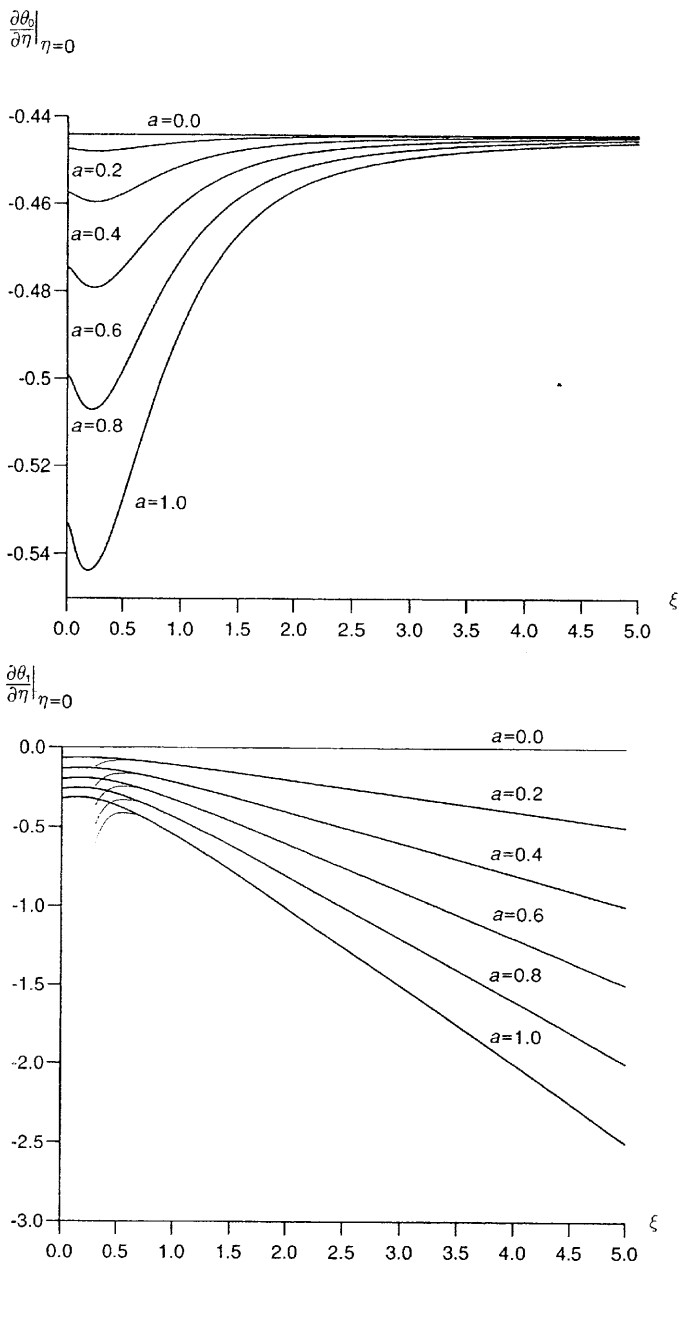

$$p^{(2)} = \tfrac{1}{2}\lambda(\eta f - \eta^2 f') \quad \text{and} \quad \theta^{(2)} = \lambda\eta f'' \tag{14}$$

where λ is an unknown coefficient. Clearly, this means that successive terms in the asymptotic series will contain parts of the solution with arbitrary coefficients. However, it remains possible to obtain exact leading-order solutions for the functions multiplying cos $2z$ and so on, even though they first appear at $O(\xi^{-5})$. We also note, in passing, that the main-layer equations admit other eigensolutions. If eigensolutions appear at $O(\xi^{-\sigma})$ in the expansion, then the first six eigensolutions correspond to the following values of σ: 2.0000, 7.6558, 17.8220, 32.5048, 51.7049, and 75.4225; these values were obtained using a fourth-order accurate Runge-Kutta shooting method code, and the values are correct to four decimal places.

Using the procedure outlined above, we find that the main-region solutions take the following forms:

$$p = h(\eta) + \xi^{-2}[\tfrac{1}{2}\lambda(\eta f - \eta^2 f')] + O(\xi^{-4}), \tag{15a}$$

$$\theta = f'(\eta) + \xi^{-2}[\lambda\eta f''] + O(\xi^{-4}), \tag{15b}$$

while the near-wall solutions are

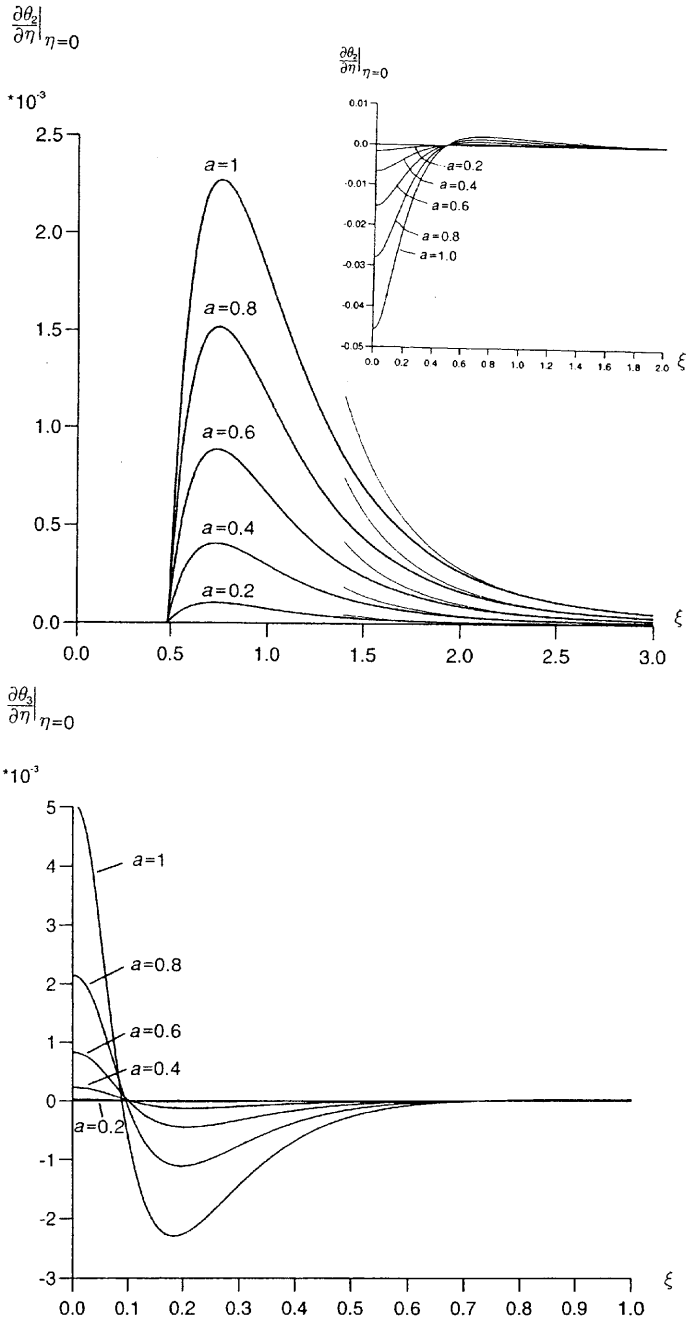

Fig. 3 The variation of the rate of heat transfer for the first few Fourier modes as functions of ξ for various surface temperature wave amplitudes: (*a*) zeroth mode; (*b*) first mode; (*c*) second mode; (*d*) third mode. The $a = 0$ curve for the zeroth mode is also the asymptotic curve for the other values of *a*. The asymptotic curves for the first and second modes are depicted as thin lines.

$$P = -\xi^{-3}\left(\frac{\gamma y^3}{12}\right) + \xi^{-5}\left[-\frac{\gamma\lambda y^3}{4} + \frac{\gamma y^5}{160} + \frac{a\gamma}{128}(y^4 + 8y^3 + 21y^2 + 21y + 21)e^{-y}\cos z\right] + o(\xi^{-5}), \tag{16a}$$

$$\Theta = (1 + ae^{-y}\cos z) + \xi^{-1}(\gamma y) + \xi^{-3}\left[\gamma\left(\lambda y - \frac{y^3}{12}\right) + \frac{a\gamma}{48}(2y^3 + 9y^2 + 9y)e^{-y}\cos z\right] - \xi^{-4}\left(\frac{\gamma^2 y^4}{48}\right) + \xi^{-5}\left[\frac{a^2\gamma}{8192}(8y^4 + 40y^3 + 6y^2 - 165y)e^{-2y}\cos 2z\right] + O(\xi^{-5}). \tag{16b}$$

In these expressions, it is to be understood that $\gamma = f''(0) \simeq -0.444$ (see (7)), the $O(\xi^{-4})$ terms in (15) are proportional to λ^2, and the $O(\xi^{-5})$ term in (16*b*) contains terms independent of z and others that are proportional to cos z. It is clear that our assumption that the main layer is independent of z is well-justified a posteriori by the inner layer results where all z-dependent terms decay exponentially into the main layer.

The above results may be used to obtain heat transfer data. In order to compare with Figs. 3, we need to obtain the η-derivative of the inner layer solutions. Thus, we find that

$$\left.\frac{\partial \Theta}{\partial \eta}\right|_{\eta=0} = (-a \cos z)\xi + \gamma + \left(\gamma\lambda + \frac{3}{16}\gamma a \cos z\right)\xi^{-2} - \left(\frac{165}{8192}\gamma a^2 \cos 2z\right)\xi^{-4} + O(\xi^{-4}). \quad (17)$$

Again, the $O(\xi^{-4})$ terms in (17) contain z-independent terms and terms proportional to cos z.

Using (17) we are able to write down the asymptotic behavior of the rate of heat transfer corresponding to the various Fourier modes defined in Eq. (8*b*):

$$\left.\frac{\partial \theta_0}{\partial \eta}\right|_{\eta=0} = \gamma + (\gamma\lambda)\xi^{-2} + O(\xi^{-4}) \quad (18a)$$

$$\left.\frac{\partial \theta_1}{\partial \eta}\right|_{\eta=0} = -\frac{1}{2}a\xi + \frac{3}{32}\gamma a\xi^{-2} + O(\xi^{-4}) \quad (18b)$$

$$\left.\frac{\partial \theta_2}{\partial \eta}\right|_{\eta=0} = -\frac{165}{16384}\gamma a^2\xi^{-4} + O(\xi^{-6}) \quad (18c)$$

$$\left.\frac{\partial \theta_3}{\partial \eta}\right|_{\eta=0} = O(\xi^{-6}). \quad (18d)$$

By considering the interaction of the nonlinear terms in Eqs. (11), it is straightforward to show that the heat transfer corresponding to mode n, the term proportional to cos nz, is of $O(\xi^{-2n})$ when $n > 1$. The expressions in (18*b*, *c*) are also shown in Figs. 3(*b*, *c*) and give very accurate comparisons with the numerical values obtained from solving the full boundary layer equations. We note that only the leading term in (18*a*) is known with certainty since λ can only be determined by a direct comparison with the full numerical solution of (9).

6 Discussion

In this paper, we have considered how the presence of longitudinal surface temperature variations affects the flow and heat transfer from a vertical heated surface in a porous medium. This is, to our knowledge, the first time a nonsimilar three-dimensional, boundary layer flow in a porous medium has been studied. The pressure and temperature fields have been determined by a combination of numerical methods and an asymptotic analysis. We have found that the flow, even for seemingly very large surface temperature waves, may be described accurately with a surprisingly small number of spanwise Fourier modes. At large distances from the leading edge, the flow is essentially the standard Cheng and Minkowycz (1977) vertical profile with only the first Fourier mode giving substantial changes from this in a near-wall layer adjacent to the heated surface. The numerical and asymptotic analyses compare very favorably, even for values of ξ as small as 3, and this lends support to the accuracy of both types of analysis.

References

Cheng, P., and Minkowycz, W. J., 1977, "Free Convection About a Vertical Flat Plate Imbedded in a Porous Medium With Application to Heat Transfer From a Dike," *J. Geophys. Res.*, Vol. 82, pp. 2040–2044.

Chiu, C.-P., and Chou, H.-M., 1993, "Free Convection in the Boundary Layer Flow of a Micropolar Fluid Along a Vertical Wavy Surface," *Acta Mechanica*, Vol. 101, pp. 161–174.

Gill, A. E., 1969, "A Proof That Convection in a Porous Vertical Slab is Stable," *J. Fluid Mech.*, Vol. 35, pp. 545–547.

Hossain, M. A., Alam, K. C. A., and Pop, I., 1996, "MHD Free Convection Flow Along a Vertical Wavy Surface With Uniform Surface Temperature," submitted for publication.

Keller, H. B., and Cebeci, T., 1971, "Accurate Numerical Methods for Boundary Layer Flows 1: Two-Dimensional Flows," *Proc. Int. Conf. Numerical Methods in Fluid Dynamics*, Lecture Notes in Physics, Springer, New York.

Kim, S. J., and Vafai, K., 1989, "Analysis of Natural Convection About a Vertical Surface Embedded in a Porous Medium," *Int. J. Heat Mass Transf.*, Vol. 32, pp. 665–677.

Kwok, L. P., and Chen, C. F., 1987, "Stability of Thermal Convection in a Vertical Porous Layer," ASME JOURNAL OF HEAT TRANSFER, Vol. 109, pp. 889–893.

Lewis, S., Bassom, A. P., and Rees, D. A. S., 1995, "The Stability of Vertical Thermal Boundary Layer Flow in a Porous Medium," *European Journal of Mechanics B: Fluids*, Vol. 14, pp. 395–408.

Moulic, S. G., and Yao, L. S., 1989a, "Mixed Convection Along a Wavy Surface," ASME JOURNAL OF HEAT TRANSFER, Vol. 111, pp. 974–979.

Moulic, S. G., and Yao, L. S., 1989b, "Natural Convection Along a Vertical Wavy Surface With Uniform Heat Flux," ASME JOURNAL OF HEAT TRANSFER, Vol. 111, pp. 1106–1108.

Nield, D. A., and Bejan, A., 1992, *Convection in Porous Media*, Springer, New York.

Rees, D. A. S., 1990, "The Effect of Long-Wavelength Thermal Modulations on the Onset of Convection in an Infinite Porous Layer Heated From Below," *Q. J. Mech. Appl. Math.*, Vol. 43, pp. 189–214.

Rees, D. A. S., 1993, "Nonlinear Wave Stability of Vertical Thermal Boundary Layer Flow in a Porous Medium," *Journal of Applied Mathematics and Physics (Z.A.M.P.)*, Vol. 44, pp. 306–313.

Rees, D. A. S., 1996, "The Effect of Layering on Free Convection From a Vertical Heated Surface in a Porous Medium," *Proc. Int. Conf. on Porous Media and their Applications in Science, Engineering, and Industry*, Kona, Hawaii, pp. 71–84.

Rees, D. A. S., and Bassom, A. P., 1993, "The Nonlinear Nonparallel Wave Instability of Free Convection Induced by a Horizontal Heated Surface in Fluid-Saturated Porous Media," *J. Fluid Mech.*, Vol. 253, pp. 267–296.

Rees, D. A. S., and Pop, I., 1994a, "A Note on Free Convection Along a Vertical Wavy Surface in a Porous Medium," ASME JOURNAL OF HEAT TRANSFER, Vol. 116, pp. 505–508.

Rees, D. A. S., and Pop, I., 1994b, "Free Convection Induced by a Horizontal Wavy Surface in a Porous Medium," *Fluid Dynamics Research*, Vol. 14, pp. 151–166.

Rees, D. A. S., and Pop, I., 1995a, "Free Convection Induced by a Vertical Wavy Surface With Uniform Heat Flux in a Porous Medium," ASME JOURNAL OF HEAT TRANSFER, Vol. 117, pp. 547–550.

Rees, D. A. S., and Pop, I., 1995b, "Non-Darcy Natural Convection From a Vertical Wavy Surface in a Porous Medium," *Transport in Porous Media*, Vol. 20, pp. 223–234.

Rees, D. A. S., and Pop, I., 1996, "The Effect of Longitudinal Surface Waves on Free Convection From Vertical Surfaces in Porous Media," *Int. Comm. Heat Mass Transf.*, in press.

Rees, D. A. S., and Riley, D. S., 1989a, "The Effects of Boundary Imperfections on Convection in a Saturated Porous Layer: Near-Resonant Wavelength Excitation," *J. Fluid Mech.*, Vol. 199, pp. 133–154.

Rees, D. A. S., and Riley, D. S., 1989b, "The Effects of Boundary Imperfections on Convection in a Saturated Porous Layer: Non-Resonant Wavelength Excitation," *Proc. Roy. Soc.*, Vol. A421, pp. 303–339.

Riahi, D. N., 1993, "Preferred Pattern of Convection in a Porous Layer With a Spatially Nonuniform Boundary Temperature," *J. Fluid Mech.*, Vol. 246, pp. 529–543.

Riahi, D. N., 1995, "Finite-Amplitude Thermal Convection With Spatially Modulated Boundary Temperatures," *Proc. Roy. Soc.*, Vol. A449, pp. 459–478.

Riahi, D. N., 1996, "Modal Package Convection in a Porous Layer With Boundary Imperfections," *J. Fluid Mech.*, Vol. 318, pp. 107–128.

Yao, L. S., 1983, "Natural Convection Along a Vertical Wavy Surface," ASME JOURNAL OF HEAT TRANSFER, Vol. 105, pp. 465–468.